JOURNAL OF GEOPHYSICAL RESEARCH, VOL. 104, NO. E11, PAGES 27,013–27,030, NOVEMBER 25, 1999

Deep Space 2: The Mars Microprobe Mission

Suzanne Smrekar,[1] David Catling,[2] Ralph Lorenz,[3] Julio Magalhães,[2]
Jeffrey Moersch,[2] Paul Morgan,[4] Bruce Murray,[5] Marsha Presley,[6]
Albert Yen,[1] Aaron Zent,[2] and Diana Blaney[1]

Abstract. The Mars Microprobe Mission will be the second of the New Millennium Program's technology development missions to planetary bodies. The mission consists of two penetrators that weigh 2.4 kg each and are being carried as a piggyback payload on the Mars Polar Lander cruise ring. The spacecraft arrive at Mars on December 3, 1999. The two identical penetrators will impact the surface at ~190 m/s and penetrate up to 0.6 m. They will land within 1 to 10 km of each other and ~50 km from the Polar Lander on the south polar layered terrain. The primary objective of the mission is to demonstrate technologies that will enable future science missions and, in particular, network science missions. A secondary goal is to acquire science data. A subsurface evolved water experiment and a thermal conductivity experiment will estimate the water content and thermal properties of the regolith. The atmospheric density, pressure, and temperature will be derived using descent deceleration data. Impact accelerometer data will be used to determine the depth of penetration, the hardness of the regolith, and the presence or absence of 10 cm scale layers.

1. Introduction

The New Millennium Program is a National Aeronautics and Space Administration (NASA) technology program with the primary goal of developing revolutionary technologies that require validation in space. The intent is to demonstrate technologies that will allow critical science to be accomplished through the development of new capabilities and reductions in mass, power, and especially, risk to future missions.

The Mars Microprobe Project, or Deep Space 2 (DS2), is the second of the New Millennium Program planetary missions. Deep Space 1 is an asteroid-comet flyby mission with the primary goal of demonstrating solar electric propulsion [*Nelson*, 1998]. DS2 is designed to enable future network missions, such as seismic or meteorology networks that require simultaneous measurements at numerous stations distributed around a planet. It will also demonstrate subsurface sample collection and analysis. To reach this objective, a highly miniaturized penetrator-based platform for in situ science has been developed. A secondary mission goal is the collection of meaningful science data.

Penetrators are instrumented devices that impact the ground at high velocity and come to rest in the subsurface due to their missile-like shape. They were first developed in the United States in the 1970s to monitor troop movement using seismometers or other instruments. The first penetrator built for a planetary mission was a large (approximately 2 m by 17 cm, with a mass of 125 kg) penetrator developed for the Russian Mars '96 mission [*Surkov and Kremnev*, 1998]. Unfortunately, the mission failed due to a launch malfunction. Japan has also developed penetrators to deploy seismometers, the main objective of its Lunar-A mission to the Moon, currently scheduled for launch in 2002 [*Mizutani*, 1995; *Garry*, 1997]. The Lunar-A penetrators have an impact mass of 12-13 kg and are intended to survive impact speeds up to 300 m/s.

DS2 will be the first planetary penetrator mission. The two identical penetrators are being carried as a piggyback payload (Figure 1) on the Mars Polar Lander (R.W. Zurek, The Mars Surveyor '98 Missions, submitted to *Journal of Geophysical Research*, 1999). Network missions require a large number of landers on the surface simultaneously, which in turn, requires that the size of the landers be minimized. The available volume for a piggyback payload on the Mars Polar Lander cruise ring placed an upper bound on the size of the aeroshell, whose final dimensions were 35 cm in diameter and 27.5 cm in height (Figure 2). These constraints led to the development of miniature systems, with a total entry mass of 3.6 kg, capable of surviving very high impact velocities and g forces, in addition to being able to operate at low ambient temperatures. Aftbody temperatures may reach as low as -80°C, and forebody temperatures could get as low as -120°C.

The probe has no parachute, rockets, or air bags to decelerate or soften its impact. The impact velocity will be in the range of 180-200 m/s. An aeroshell orients the probes to impact nearly vertically and provides a protective heat shield. The aeroshell is carried all the way to the ground and shatters at the surface. On impact, the penetrator separates into two parts: an aftbody that remains at the surface due to its larger diameter

[1]Jet Propulsion Laboratory, California Institute of Technology, Pasadena.
[2]Space Sciences Division, Ames Research Center, Moffett Field, California.
[3]Lunar and Planetary Laboratory, University of Arizona, Tucson.
[4]Department of Geology, Northern Arizona University, Flagstaff.
[5]Division of Geological and Planetary Science, California Institute of Technology, Pasadena.
[6]Department of Geology, Arizona State University, Tempe.

Paper number 1999JE001073.
0148-0227/99/1999JE001073$09.00

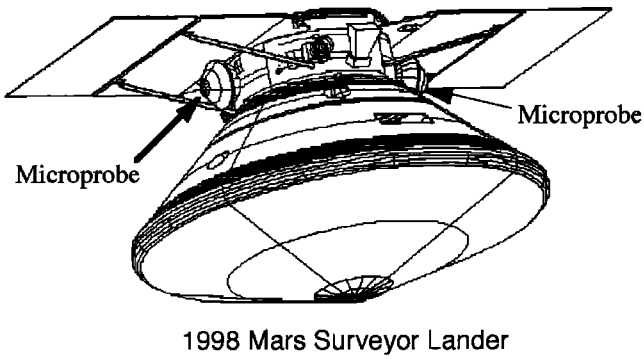

Figure 1. Mars Polar Lander and Mars Microprobe cruise configuration.

and a forebody that plunges beneath the surface due to its narrow, bullet-like shape and the high impact velocity (Plate 1). The forebody will experience up to 30,000 g (in this paper, g refers to the average acceleration of gravity at the surface of the Earth, 9.8 m/s^2) and penetrate between 0.2 and 0.6 m, depending primarily on the ice content of the soil. The aftbody deceleration will be up to 60,000 g. The aftbody comes to rest in a crater roughly 0.5 m in diameter by 0.1 m deep. A 1 m tether that relays the power and the data connects the two sections of the probe.

DS2 will carry out four science investigations. The basic science objectives are (1) to derive the atmospheric density, pressure, and temperature throughout the entire atmospheric column; (2) to characterize the hardness of the soil and possibly the presence of layers at a scale of tens of centimeters; (3) to determine if ice is present in the subsurface soil; and (4) to estimate the thermal conductivity of the soil at depth. The atmospheric density, pressure, and temperature can be derived from the deceleration during atmospheric entry, measured by an accelerometer. A second accelerometer will measure the deceleration during impact. These data will be used to estimate the depth of penetration, the hardness of the regolith, and determine whether there are significant layers with strong material property contrasts. Once part of the probe has come to rest at a depth between 30 and 60 cm, a drill will extract a small soil sample, heat the sample to 10°C, and look for the presence of water vapor using a tunable diode laser. Two temperature sensors in the forebody will monitor the rate at which the probe cools. The soil thermal conductivity will be estimated by comparing the observed cooling rate on Mars with calibrated models of the probe cooling.

Because of the rapid, 3-year development time for DS2 and the highly integrated nature of the penetrator design, the instrument development schedule was extremely tight. Instruments could not be developed in parallel with the penetrator and delivered as individual components. Instead, each instrument design progressed in parallel with the penetrator design, with each component needing to survive high-speed impact tests in order to qualify and be integrated into the design. The science team was selected once instrument designs were complete and fabrication was under way. One of their primary functions is to carry out instrument characterization work on engineering instrument models to maximize the science value of the data to be returned from Mars. The present state of this work is described in this paper.

The DS2 project got its start in December of 1995 and has a total cost of $28.2 million (M), including $0.9 M for operations and $1.1 M for launch vehicle integration. Another $1.2 M covers science team activities. This mission will validate numerous new technologies and expects to collect important science data. However, the ultimate success of the mission lies in the future science missions that may be enabled by the numerous new technologies, which include an innovative single-stage entry system, low-temperature batteries, and microelectronics designed for high-speed impacts [*Gavit and Powell*, 1996]. Atmospheric pressure sensors [*Reynolds et al.*, 1998] and seismometers [*Banerdt et al.*, 1993; *Pike et al.*, 1996] for network science have already been developed that can fit within the DS2 size constraints and withstand the impact forces. In addition, concepts for a wide range of measurements are under development for the DS2 platform [*Yen et al.*, 1999]. This paper describes the mission, the science investigations that will be carried out, and their relationship to other Mars missions and science objectives.

2. Mission Overview

The Polar Lander, with DS2, was launched on January 3, 1999, on a Delta II (7425) rocket and will arrive at Mars on December 3, 1999. The DS2 probes are powered off during cruise. Five minutes before entering the atmosphere, the release of the Polar Lander from its cruise ring will cause the microprobes to be jettisoned and the batteries and computer to power up. During entry, the probe collects deceleration data and checks out all systems prior to impact ~ 12 min later. The two probes will land ~ 50 km northwest of the lander and up to10 km from each other. Because of their higher speed in the lower atmosphere, the probes arrive at the surface prior to the lander.

The probes and the Polar Lander are expected to impact on the south polar layered terrain. The polar layered terrains are believed to be alternating layers of aeolian deposited dust and

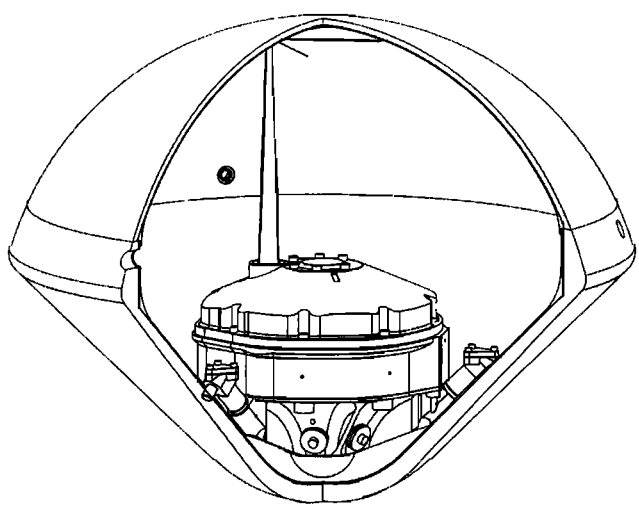

Figure 2. Cut away view of the Mars Microprobe in the cruise configuration. The forebody sits inside the aftbody. Both are stowed in the nose of the aeroshell. The conical portion of the aeroshell is the heat shield. The aftbody dimensions are 136 mm in diameter and 105 mm in height, plus the 127 mm antenna. The mass is 1.737 kg. The forebody has a diameter of 39 mm and a length 105.6 mm. The mass is 0.67 kg.

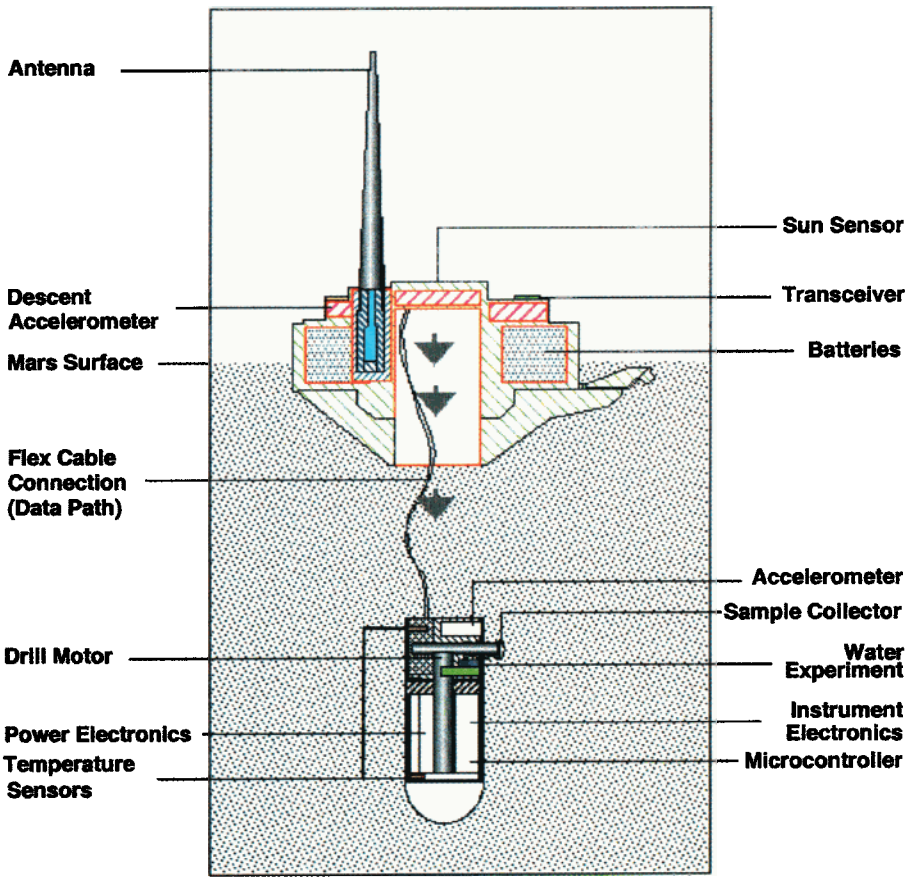

Plate 1. Locations of the major probe components.

volatiles condensed from the atmosphere and may thus record changes in the Martian climate (D. A. Paige et al., The Mars Volatiles and Climate Surveyor (MVACS) integrated payload for the Mars Polar Lander; A. R. Vasavada et al., Surface properties at the Mars Polar Lander landing site, submitted to *Journal of Geophysical Research*, 1999; hereinafter referred to as submitted papers). Unless further data from MGS cause the landing site to be reevaluated, the center of the 200 by 20 km DS2 landing ellipse is located at 75.3°S, 195.9°W. The probes will arrive in late spring in the southern hemisphere, ~1 month after the retreat of the seasonal CO_2 frost cover. The location of the probes will be estimated after impact using Doppler shifts in the communications signal to determine the range of possible locations. The location accuracy will be between hundreds of meters and several kilometers, depending on the number of transmissions and the geometry of passes.

The nominal mission lifetime is one Martian day. Most of the mission data are collected the first day and relayed to the Mars Global Surveyor (MGS) orbiter. Additional soil temperature data will be collected and transmitted for as long as the batteries last, possibly up to 1 week. Data collection begins as soon as the probes are powered on, following separation from the lander cruise ring. Once the battery voltage stabilizes, the two computers (one in the aftbody and one in the forebody) will collect engineering data from all systems, including check outs of the instrument sensors and electronics. The descent accelerometer is sampled at 20 Hz during entry. Approximately 100 s before impact, sampling of the impact accelerometer at 25 kHz begins. Following impact, the forebody soil conductivity sensors are initially sampled once every 30 s to monitor the cooling history of the probes. This sampling rate gradually decreases, so that after the first hour the sampling rate becomes once every 30 min for the duration of the mission. Currently, two transmissions of data to the orbiter are scheduled for each of the first two days, followed by once a day for the remainder of the mission. The water experiment sequence runs following the first successful transmission of the data.

3. Polar Layered Terrain and the DS2 Test Program

The polar layered terrains of Mars are believed to be composed of layers of dust and ice whose deposition and modification have been controlled by the climate and geologic history of Mars [e.g., *Thomas et al.*, 1992]. The exact water and dust content of the deposits cannot be accurately determined based on remote sensing data. Although the topography of the polar layered deposits is being accurately determined by the Mars Observer Laser Altimeter [*Ivanov and Muhleman*, 1999] on MGS, the trade-off between temperature and dust content means the dust abundance cannot be accurately calculated [*Zuber*, 1999].

The available information on the physical properties of the near-surface materials suggests that it could be anything from very fine grained aeolian dust to frozen ground with a high ice content. At the low Martian temperatures and high impact ve-

locities predicted for DS2, frozen ground is nearly as hard as rock. Analysis of the color and albedo of the polar deposits from Viking data indicates that the layered terrains consist of three components: bright dust, ice, and a small amount of dark material [*Herkenhoff and Murray*, 1990a]. The large lateral extent and constant thickness of the layers indicate that they were deposited from atmospheric suspension. Recent data from the Mars Pathfinder camera indicate that the suspended haze particle size is approximately 1 μm [*Smith et al.*, 1997]. The bright material is similar to the red dust observed over much of the planet [*Herkenhoff and Murray*, 1990a]. *Herkenhoff and Murray* [1990a] interpret the minor quantities of dark material to be sand-sized particles based on the distribution of the dark material. This material forms dune fields in places, indicating transport via saltation. Estimates of surface slopes of up to 20°, based on photoclinometry and stereophotogrammetry, suggest the presence of a competent weathering rind [*Herkenhoff and Murray*, 1990b]. This weathering rind is interpreted to be the source of the sand-sized particles (~100 μm) and could be created by sublimation of dust and ice mixtures. An alternative explanation, based on thermal inertia data for similar deposits near the north pole, is that the dark material may be fine sand-sized grains [*Paige et al.*, 1994]. The absence of ice flow features indicates that the ice content likely is less than 40% by volume [*Hofstadter and Murray*, 1990]. A more complete review of the physical properties of the south polar layered terrain and the latest analysis of thermal inertia data from MGS can be found in the work by A. R. Vasavada et al. (submitted paper, 1999).

Numerous factors indicate that ice is not present at the immediate surface, including color and albedo [*Herkenhoff and Murray*, 1990a], but is likely at shallow depths. Thermal inertia data indicate extremely low conductivity in the upper several millimeters of the deposits [*Paige and Keegan*, 1994], consistent with aeolian deposition. The observed Earth-based 3.5 cm radar returns from south polar layered deposits indicate that the dust layer at the surface cannot be more than tens of centimeters thick [*Muhleman et al.*, 1991]. Models of the stability of water ice at the poles indicate that ice is likely to occur at depths as shallow as 4-20 cm [*Paige*, 1992]. The depth of penetration thus was constrained to be a minimum of 30 cm, to ensure that the drill would sample regions in which ice is predicted.

More recent data from the Mars Orbital Camera on board the MGS spacecraft shows that layers are present down to the current limit of the resolution (~2-3 m) in the polar layered terrains (Malin Space Sciences Web site). The relatively low resolution thermal inertia data available to date from the Thermal Emission Spectrometer on MGS are globally consistent with past observations [*Mellon et al.*, 1999; B. M. Jakosky et al., The thermal inertia of Mars from the Mars Global Surveyor Thermal Emission Spectrometer, submitted to *Journal of Geophysical Research*, 1999].

The possible range of hardnesses of the near-surface polar layer deposits presented a challenge to both the design and testing of the microprobe. A major element of the project development was the testing of components and systems for impact survivability. Early tests of the mechanical design were conducted using airplanes to drop test prototypes at appropriate velocities. Later tests of more high-fidelity components and designs were carried out in conjunction with Sandia National Laboratories at the New Mexico Institute of Mining and Technology's Energetic Materials Research and Test Center in Socorro, New Mexico. The air gun facility rests on an 18-wheeler truck and has a length of 5.5 m and a diameter of 15 cm. More than 60 air gun tests were conducted to verify the performance of all systems. The target material most frequently used to verify impact survivability was native clay.

Depth of penetration tests were performed in a variety of materials to represent the possible range of conditions likely in the polar layered deposits. In the weapons community, penetrator targets are described by an empirical parameter called the penetrability parameter, or simply the "S value" [*Young*, 1997], a measure of the target's resistance to penetration. The S value of a target material is inversely related to the number of blows needed to drive a penetrometer into the material to a particular depth; typical "hard" materials have S values of 1-5, and "soft" materials have S values of 15 or more. Air gun experiments are used to determine a penetrator's performance into different known target materials with a range of S values. The penetrability of an unknown target, such as the Martian surface, can be determined by comparing the depth of penetration measured by accelerometry with that expected for various S numbers. Tables of S values have been compiled for a large variety of target materials [*Young*, 1997], some of which are duplicated in the impact accelerometer experiment section of this paper. Air gun tests of the DS2 penetrator design were carried out in fine-grained (~100 μm) sand with an S number of ~10-15, in hard-packed sand with a particle size of ~150 μm and an S of ~5, and in frozen targets with an S as low as 1. Maintaining large frozen targets at -40°C in New Mexico in July posed logistical difficulties, and therefore such targets were used only twice. However, these tests did demonstrate the ability of the probes to penetrate into ice and survive the impact. A separate air gun facility at Eglin Air Force Base in Fort Walton Beach, Florida, was used to test the performance of the aeroshell design. Tests with the 6 m long, 38 cm diameter air gun proved that the aeroshell shatters on impact and allows the probe to penetrate the surface. The aerodynamic characteristics of the aeroshell were determined in tests at both Eglin Wright Laboratory Ballistic Range and at a supersonic wind tunnel in Kalingrad, Russia, which simulated the Reynolds number regime appropriate for Martian atmospheric pressures.

4. Science Investigations and Instrument Descriptions

4.1. Atmospheric Structure Investigation

4.1.1. Science objectives. Measurements of the deceleration history of an atmospheric entry probe can be used to derive the variation of atmospheric density, pressure, and temperature along the probe's trajectory through the atmosphere [*Magalhães et al.*, 1999; *Seiff and Kirk*, 1977]. Mars Microprobe Atmospheric Descent Accelerometer (ADA) data will be used to derive such atmospheric structure profiles along the trajectories of each of the microprobes from ~ 75 km altitude down to the surface. These data will provide the first atmospheric structure observations of the polar regions (~75°S latitude versus 19.1°N for Pathfinder, 22.3°N for Viking 1, and 47.6°N for Viking 2) and the first atmospheric structure measurements in the southern hemisphere. The microprobes thus will provide a unique opportunity to investigate polar atmospheric structure and place observational constraints on the dynamics of the polar atmosphere. The late southern spring season (L_S=259°) of

the entries will probe a quite different season than previous landers, which have all entered during northern summer, and thus will provide observational constraints on the dynamics at this season. The two Mars microprobes, which will enter the Martian atmosphere nearly simultaneously and will impact the surface separated by a 10 km, will also provide the first opportunity to study the horizontal variability of local atmospheric structure over this length scale.

The relative contributions of different dynamical processes to the atmospheric circulation and structure of the polar regions is poorly constrained, and detailed observations of the thermal structure and water vapor distribution could provide useful information to constrain modeling efforts [*Pollack et al.*, 1990]. Understanding the dynamics of the polar regions is critical to assessing the water and dust cycles on Mars, since the dynamics govern the exchange of volatiles and dust between the polar regions and low latitudes [*Jakosky and Haberle*, 1992]. General circulation model results [*Haberle et al.*, 1993] suggest the microprobes will arrive in a region influenced by a circulation resulting from the temperature contrast between the cold residual cap and the warm surrounding terrain, analogous to a sea-breeze circulation. In addition, at the season of arrival, atmospheric dust levels will likely be increasing from the background levels studied during previous atmospheric entries, and the atmospheric pressure will be near its annual maximum [*Zurek et al.*, 1992].

Due to the in situ nature of the measurement and the resulting high spatial resolution, the atmospheric structure profiles from the Mars microprobes will provide unique information on atmospheric processes with vertical and horizontal scales smaller than 10 km. Atmospheric waves such as gravity waves with wavelengths in this range can be identified. Such waves can directly perturb the thermal structure and circulation and can also indirectly influence the atmosphere through the momentum and energy they transport vertically and meridionally [*Barnes*, 1990]. Convection and turbulence associated with unstable or neutral temperature lapse rates is potentially detectable. Atmospheric layers that are saturated with respect to carbon dioxide and water vapor can be identified and potentially associated with cloud or fog formation. The effects of aerosol layers (dust and condensates) also are potentially detectable in the temperature profile through their influence on direct solar heating and radiative cooling [*Haberle et al.*, 1999]. Thus the observations from the ADA provide a valuable opportunity to make in situ measurements of atmospheric structure in the polar regions over a broad altitude range and to study the role of small-scale atmospheric processes in the polar atmosphere.

4.1.2. Instrument description. The ADA is mounted in the aftbody of the microprobe and is aligned parallel to the entry vehicle's axis of symmetry (z axis) at a radial distance from the z axis of about 25 mm. The ADA measures acceleration parallel to the z axis only. The Mars Microprobe ADA is an Analog Devices ADXL250aqc unit. This device senses acceleration by measuring the capacitance between fixed plates and moveable plates that are elastically attached to the substrate of the device. Under the influence of an applied acceleration, the moveable plates are displaced until the elastic force balances the applied acceleration. The change in the plate position and hence the capacitance provides a measure of the applied acceleration. All of the circuitry needed to drive the sensor and convert the capacitance change into an output voltage is included in the 5 g highly integrated circuit of this surface micromachined device. The accelerometer has a range of -25 to 25 Earth g. Output voltage from the ADA is digitized to 11 bits by an application specific integrated circuit (ASIC) to yield a digital resolution of 38 mg/ count (mg refers to milligravity units = 9.8 x 10^{-3} m s^{-2}). Sampling and storage of data from the ADA is controlled by the telecommunication system of the microprobe. Data from the probes will be sampled at ~20 Hz, starting ~ 60 s before atmospheric entry and ending at impact.

The ADXL250 is an off-the-shelf microaccelerometer that has been used in a wide range of civilian and military applications including automobile air bags and howitzer shells. The manufacturer, Analog Devices, has extensively studied the performance of the units and compiled statistics on their characteristics based on testing of a large fraction of the units that have been assembled and shipped. Test results from the manufacturer span the temperature range -40°C to +85°C, which includes the nominal expected probe temperature prior to atmospheric entry (-36°C) and the expected small internal heating associated with the atmospheric entry. Noise levels of a few mg in the 0-100 Hz frequency range are well below the digital resolution of the experiment. The manufacturer's statistics show a spread of up to ±3% (1 standard deviation) in the scale factor of the units. Scale factor drift of 0.01%/°C and zero offset drift of 5 mg/ °C is indicated by the data as well. Nonlinearity is typically ~0.2% of full scale. A flight spare unit has been tested, and its characteristics are consistent with the manufacturer's specifications. Unfortunately, no calibration data for the flight units were acquired; however, as we discuss below, independent observations of the surface atmospheric density and the altitude of the probe impact site will provide a tight constraint on the scale factor of the flight units. Calibration data on the flight unit ASICs define the transfer function of the analog-to-digital converter for the ADA. The relative timing between the ADA measurements is controlled by the telecommunications system's oscillator frequency whose drift with temperature has been measured.

4.1.3.Experiment description. Atmospheric density ρ is related to the aerodynamic deceleration of a spacecraft through the aerodynamic drag equation:

$$\rho = -\frac{2m}{C_D A}\frac{a_v}{V_R^2} \quad (1)$$

where a_V is the acceleration along the flight path relative to the atmosphere, V_R is the probe velocity relative to the atmosphere, m is the probe mass, C_D is the drag coefficient of the probe, and A is the probe's cross-sectional area. The drag coefficient C_D varies during the entry, and this variation can be accounted for iteratively using aerodynamic databases compiled from preflight experiments and numerical simulations. For the Mars microprobes, m/C_DA ~ 38 kg m^{-2}. The velocity and position are derived by integrating over time the equations of motion of the vehicle using the measured aerodynamic deceleration and knowledge of the gravity field [*Magalhães et al.*, 1999]. Trajectory solutions for the approach of the microprobes, to Mars will be generated by the Mars Surveyor navigation team and will provide an initial condition for the trajectory integration. Atmospheric pressure versus altitude is derived by integrating the density profile using the equation of hydrostatic equilibrium. The ideal gas law along with a model for the molecular weight variation in the Martian atmosphere then is used to derive atmospheric temperatures.

As can be seen from (1), deceleration along the flight path is needed to derive the atmospheric structure, but the ADA measures acceleration along the z axis only. The microprobes will enter the atmosphere at an unknown angle of attack (angle between velocity vector and z axis of the probe) with unknown angular rate <30°/s. The aeroshell shape and mass distribution have been chosen so that aerodynamic torques in the upper atmosphere will reorient the vehicle to a small angle of attack by the time of peak deceleration and peak aerothermodynamic heating at 40-50 km altitude. Figure 3 presents the acceleration along the z axis from a six-degree-of-freedom simulation of the Mars Microprobe entry by *Braun et al.* [1999]. Such simulations (note the ripple in Figure 3) and the theory of the angular motions of an entry vehicle show that the angle of attack oscillates about zero with decreasing amplitude and increasing frequency as the dynamic pressure, which is proportional to the atmospheric density, increases. Analytical expressions for the form of the oscillations derived from the simulations and the theory will be used to invert the z axis acceleration measurements and derive the total angle of attack and deceleration along the flight path as a function of time.

For m/C_DA appropriate for the microprobes, the entry velocity of ~7 km/s, and the 38 mg digital resolution, (1) indicates the ADA will begin sensing the atmosphere at ρ~5 x 10-7 kg m-3. Based on the Viking and Pathfinder entry profiles with a correction for the annual surface pressure variation of the Martian atmosphere, the threshold density corresponds to atmospheric detection at an altitude of about 90 km and to 10 counts at 75 km altitude. The vertical resolution of the profiles based on the vertical velocity of the microprobe, the angle of attack oscillation frequency, and the sampling frequency should vary between ~1 km at the start of the profile to ~100 m as the surface is approached. The total probe accelerations after the deceleration peak in Figure 3 remain well above the acceleration of gravity until impact with the surface. Therefore this indicates the probe continues decelerating due to atmospheric drag and does not achieve a balance between aerodynamic drag and the force of gravity (equilibrium descent) prior to impact. Since the microprobe remains within its aeroshell until impact, the microprobes will for the first time permit the use of accelerometer data to reconstruct atmospheric structure down to the surface of Mars. Previous landers have required pressure and temperature sensors to evaluate atmospheric structure below about 8 km during their parachute descent phases [*Seiff and Kirk*, 1977].

Probe velocity and flight path angle below horizontal (angle between velocity vector of probe and the local horizontal) from the entry simulations of *Braun et al.* [1999] are displayed in Figure 4. Note that the impact velocity is predicted to be between 160-200 m/s and is strongly affected by the altitude of the impact site. The large velocities throughout entry, descent, and impact are well above predicted atmospheric winds so that the atmospheric structure analysis is relatively insensitive to the effects of winds. The flight path angle for an impact at 1 km altitude is ~80°, resulting in an incidence angle of ~10° for a level surface. Throughout most of the entry, the flight path an-

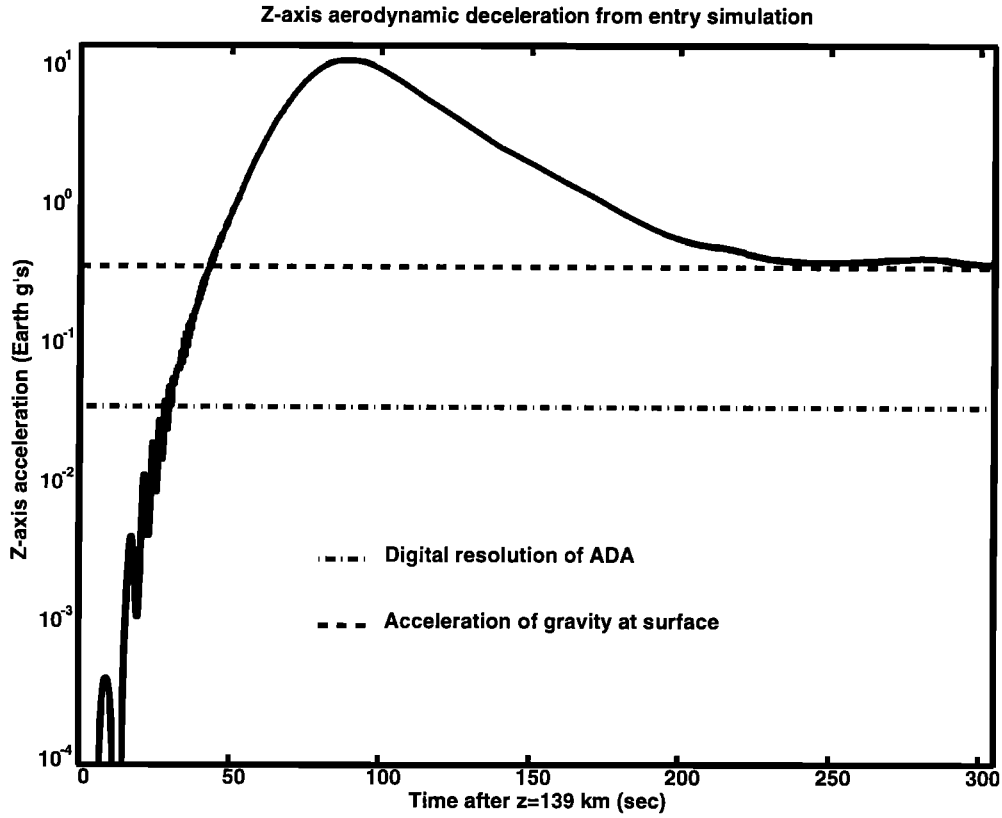

Figure 3. Aerodynamic deceleration along the z axis of the Mars Microprobe from entry simulation by *Braun et al.* [1999]. The digital resolution of the ADA and the surface acceleration of gravity have been plotted for comparison as well. Figure 5. Probe velocity and flight path angle below horizontal from entry simulations by *Braun et al.* [1999]. Flight path angle below horizontal is the angle between the velocity vector of the probe and the local horizontal.

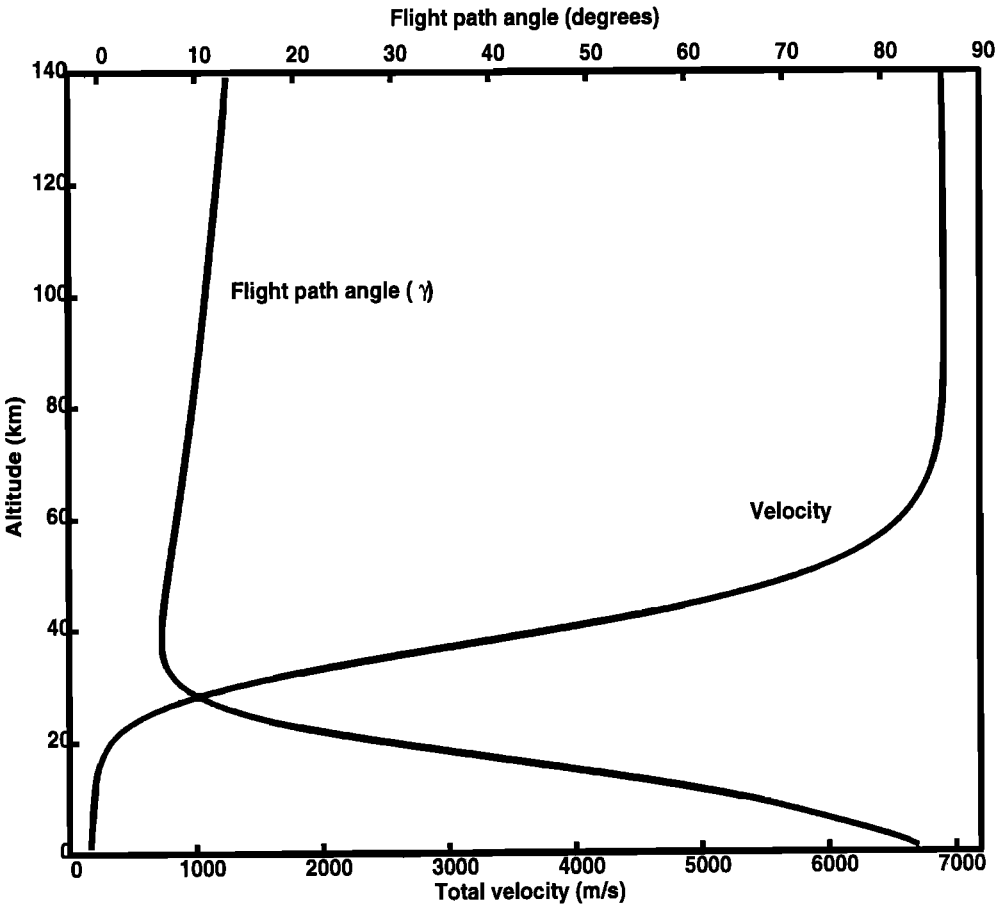

Figure 4. Probe velocity and flight path angle below horizontal from entry simulations by *Braun et al.* [1999]. Flight path angle below horizontal is the angle between the velocity vector of the probe and the local horizontal.

gle is well below 80° so that significant horizontal motion of the probe occurs during the traverse of the atmosphere.

Uncertainties in the atmospheric structure profiles will be governed by different factors during the course of the entry. Two key concerns are the uncertainty in the absolute time at which ADA observations are made and the value of the scale factor of the accelerometers. The relationship between spacecraft clock time and universal time is unknown to within 50 s due to uncertainty in the time required for the battery voltage to reach its nominal value and due to the lack of tie points between the spacecraft clock and events for which an absolute time is known. As a result, an unknown offset is introduced between the start time of the deceleration history measured by the ADA and the known absolute time of the initial entry velocity provided by the Mars Surveyor navigation team. This uncertainty significantly affects the position (altitude, latitude, longitude) assigned to the measurements throughout the entry and has a noticeable effect on the derived atmospheric density, pressure, and temperature after the deceleration peak (below ~40-50 km). The scale factor uncertainty has a monotonically increasing and strong effect on the error in the density, pressure, and temperatures after the deceleration peak (below ~40 km). Physically, this strong effect after the deceleration peak is due to the large decrease in velocity which controls the relationship between measured deceleration and derived density as shown in (1).

Figure 5 illustrates the sensitivity of the impact altitude, surface atmospheric density, and impact velocity to uncertainties in the absolute time and the scale factor. These results were generated by introducing errors in absolute time and scale factor into the reconstruction of a deceleration history generated from an entry simulation through a known atmosphere. The strong sensitivity of the derived surface density and impact velocity to the scale factor error and the relatively weak dependence on the timing uncertainty indicate that an independent measurement of the surface atmospheric density or impact velocity provides a means of accurately determining the scale factor of the flight unit accelerometers. We will use measurements of the surface atmospheric density from the Mars Polar Lander's Meteorology Experiment (D. Crisp et al., The meteorology instrument for the Mars Polar Lander Mars Volatile and Climate Surveyor payload, submitted to *Journal of Geophyical Research*, 1999; hereinafter referred to as submitted paper) to accurately determine the scale factors of the ADAs and thus to significantly increase the accuracy of the atmospheric structure profiles below ~40 km altitude. Determination of the landing site altitude by Doppler tracking of the radio signal from the Mars microprobes will then be used to accurately determine the relationship between spacecraft clock time and universal time. This determination will permit accurate altitudes to be assigned to the measurements and will allow further refinement of the atmospheric structure profiles.

Additional uncertainties in the analysis include the angular alignment of the ADA with the z axis, uncertainty due to the digital resolution, uncertainty in the aerodynamic properties of the microprobes, and uncertainties in the

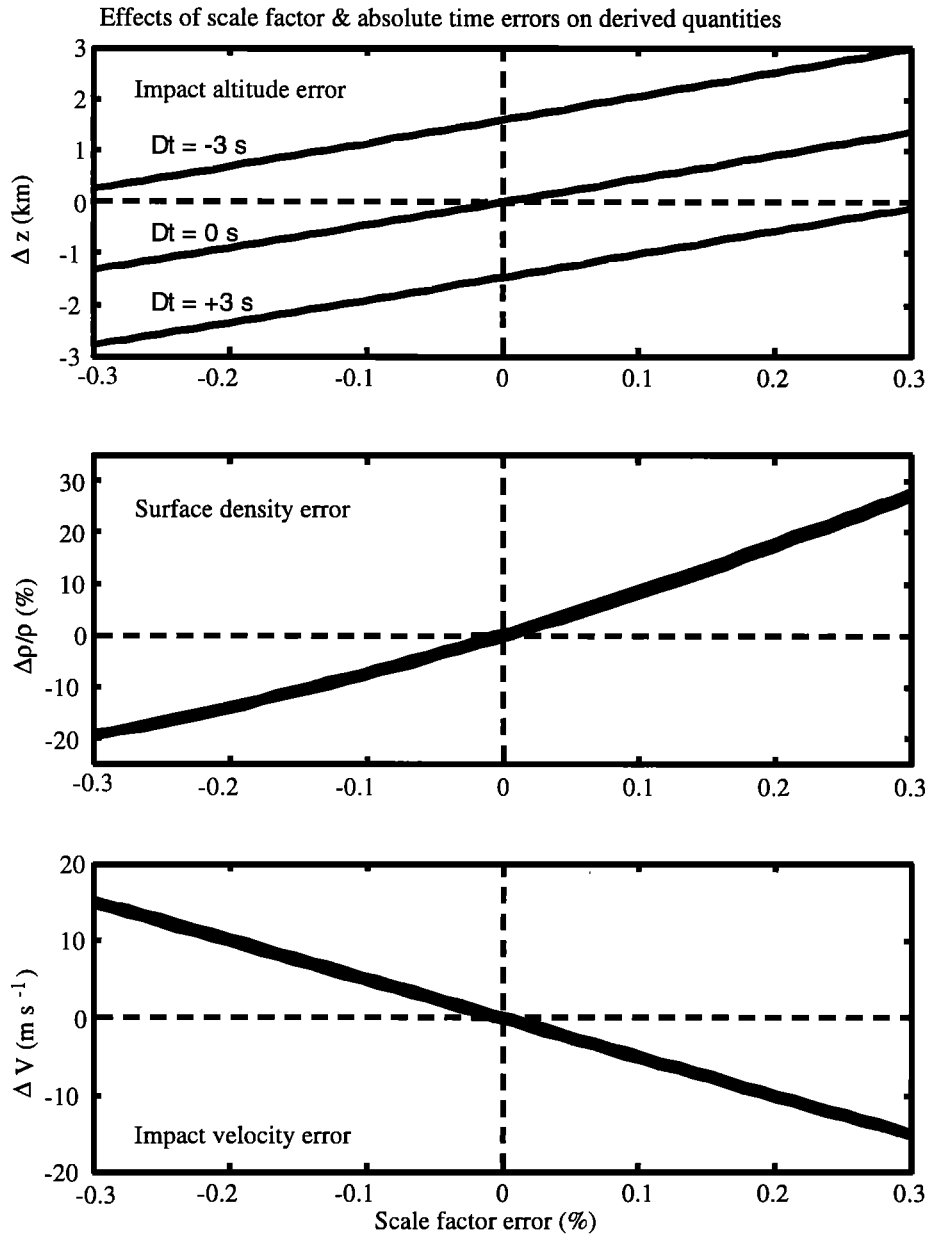

Figure 5. Effects of descent accelerometer scale factor error and absolute time error on quantities derived from atmospheric descent deceleration measurements. Derived impact altitude error, surface density error, and impact velocity error are plotted as functions of the error in the accelerometer's scale factor. In each subplot the errors are plotted for three values of the offset between spacecraft clock time and true universal time (UT); Δt = 0 s corresponds to assigning the correct UT to the zero of the spacecraft clock and hence to assigning the correct initial entry velocity to the trajectory integration. Similarly, Δt = +3 s corresponds to assigning spacecraft clock time to a UT that is 3 seconds later than the true UT. Note the strong dependence of the derived surface density and impact velocity on the scale factor error and the relatively weak dependence of these derived quantities on the absolute time errors; in the lower two plots the three lines overlay each other. Independent determinations of the surface atmospheric density and/or impact velocity thus provide a powerful means of refining our knowledge of the descent accelerometer's scale factor. Independent determination of the impact altitude can then be used to derive the correct relationship between spacecraft clock time and UT. Thus measurement of the surface atmospheric density by the Mars Polar Lander Meteorology experiment and determination of the impact locations by Doppler tracking of the DS2 radio signal will provide a powerful basis for increasing the accuracy of the atmospheric structure profiles.

temperature dependence of the ADA and associated electronics. Any error in the alignment will be indistinguishable from error in the scale factor of the accelerometer; the procedure described earlier to solve for the scale factor will account for errors in the ADA alignment as well. Digitization uncertainty will be minimized by filtering the ADA observations with a low-frequency-pass filter, which will effectively occur when we solve for the angle of attack and deceleration history, as described earlier. By applying the atmospheric structure profile reconstruction procedure to digitized and low-pass filtered deceleration histories computed from entry simulations into the atmospheric structure found by Viking 1, we find that all the major structures observed by Viking 1 in the middle and lower atmosphere could be observed with the microprobe measurements. Aerodynamic drag coefficient uncertainties [*Mitcheltree et al.*, 1999] introduce 1-3% error in the atmospheric density and pressure, depending on the flight regime; uncertainty in the temperature is smaller and depends on the time scale over which the drag coefficient varies. ADA data will be collected prior to atmospheric detection, and these data will provide a good measure of the zero-*g* bias level of the ADA, thus facilitating detection of the atmosphere. The internal temperature of the microprobes is expected to be reasonably constant during the entry, descent, and impact phase (EDI) so that the variation with temperature of the characteristics of the ADA and associated electronics should be small, accountable via a linear temperature dependence, and lead to only a small contribution to the uncertainties in the final result.

4.2. Impact Accelerometer Investigation

4.2.1. Science objectives. The deceleration history of a projectile may be used to infer the strength and homogeneity of the target material. For the polar layered terrain, the objective is to translate accelerometer data into information on the presence or absence of 10 cm scale layers and their volatile content. The higher the volatile content, the harder the layer. Information derived from the accelerometer data on hardness will be compared with data from DS2 and the Polar Lander on water content.

4.2.2. Instrument description. The impact accelerometer hardware in each of the two DS2 microprobes consists of a uniaxial accelerometer mounted inside the forebody of the probe, aligned with the long axis of the probe. The accelerometer is a ruggedized piezoresistive design (Endevco Model 7570A) with a measurable input range of −10,000 *g* to 30,000 *g* and a precision of 10 *g*. The accelerometer is polled by the probe's advanced microcontroller at a sampling rate of 25 kHz, starting ~100 s before impact and ending when the probe forebody comes to a halt. Due to data volume limitations, only the final 30 ms of accelerometer data (which will encompass the entire impact event) are stored for later transmission.

4.2.3. Experiment description. The interpretation of the accelerometer data may be conveniently considered in two distinct parts. First is how the telemetered data relate to the kinematics of the vehicle during its "lithobraking" phase, and second is how the mechanical properties of the surface relate to the kinematics.

The first element is essentially an exercise in error propagation. The sensed parameter, namely, the amplified voltage across the micromachined silicon bridge, is potentially contaminated by nonlinearities and noise in the signal chain (amplifiers, A/D conversion) and depends not only on the longitudinal acceleration of the vehicle, but also on the voltage used to excite the bridge. Since the accelerometer is slightly off-axis, rotational accelerations can further contaminate the signal, as can lateral accelerations. Lateral accelerations, especially in the first part of the impact, can be comparable with the longitudinal ones [*Young*, 1992], and like most accelerometers, the sensor flown has a cross-axis sensitivity of about 0.5%.

We will simulate these effects with a computer code, the Integrating Mars Penetrator Accelerometer Testbed (IMPAcT). This is a modified version of a code written by Moersch in support of the Comet Rendezvous / Asteroid Flyby mission. Its purpose is to simulate the performance of accelerometers on a penetrator, integrate the simulated or actual flight accelerometer data, and produce a record of the derived penetrator path. IMPAcT treats six degrees of freedom (*x, y, z,* and yaw, pitch, and roll) and is capable of simulating errors associated with accelerometer positioning and alignment, quantization and aliasing from sampling rates, *g* resolution, random electronic noise, and filtering in the spectral domain. Of course, since we have a measurement in only one of these 6 degrees of freedom, we derive only bounds on the actual trajectory. However, with estimates of the impact velocity and angle, and reasonable expectations of only modest rotations during the impact event, the essential kinematics should be correctly reconstructed. A direct product of this stage of the data analysis is the determination of the achieved depth of penetration and error estimates therein. In addition to providing a starting point for the analyses of material properties of the surface (see below), these results will also be used in the interpretation of results from the thermal conductivity and water detection experiments onboard the penetrator forebodies.

The second element of the interpretation process is rather more complicated, namely how the measured deceleration depends on impact conditions, penetrator mass and shape, and most importantly target material properties. A commonly used approach in the military arena is to bundle all material properties into a single dimensionless parameter, the "penetrability index" *S*. The *S* number in general correlates with broad soil categories, with a hard material like frozen soil having an *S* number of 2-4, while easily penetrated loose sand or dust deposits might have an *S* number greater than 20. Figure 6 shows the penetration depths expected for the DS2 penetrators into materials with a range of different *S* values.

The canonical penetration equations [*Young*, 1997], developed for the Earth Penetrating Weapon Program, indicate that penetration depth is proportional to *S*, although the caveat must be made that these equations were developed for projectiles rather larger than DS2.

As described above, a series of more than 60 engineering tests on the DS2 penetrators were conducted at the Energetic Materials Research Test Center (EMRTC) in Socorro, New Mexico, to verify correct and reliable emplacement [*Stone and Rivellini*, 1998] of the microprobes (both forebody and aftbody) under a variety of soil types and impact speeds, and to determine the survivability of various components such as the crystals in the telecom system and the motor for the sample acquisition drill.

These tests used a 6 inch diameter air gun built by the Sandia National Laboratory. The microprobe is placed in a foam sabot (shaped to provide the desired angle of attack, the

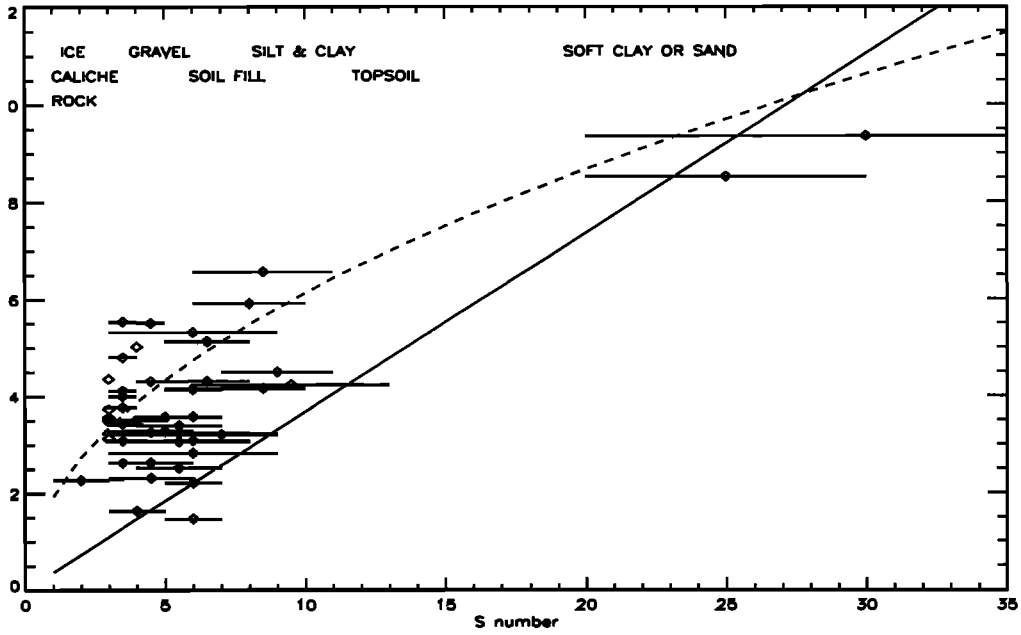

Figure 6. Expected penetration depth, assuming impact velocity of 200 m/s and forebody mass of 850 g as a function of soil hardness *S*. Solid line is formula by *Young* [1967; 1997]; dashed line is that in the text. Diamonds with error bars indicate results from New Mexico tests. Upper part of graph indicates typical soil types associated with various *S* number ranges.

angle between the velocity vector and the normal to the surface) inside the gun. The gun is pumped to high pressure until a burst disk fails and projects the microprobe into the target material. X-ray flash photography and streak cameras are used to verify the angle of attack and velocity. The target material was frequently New Mexico native clay, although some planetary analogs (ice, sand, etc.) were used.

Historically, since it is easier to disinter a projectile and measure its penetration depth than to record its deceleration history, the penetration depth is the parameter predicted. An empirical study [*Lorenz et al.*, 1999] of the New Mexico data for DS2 found that a good agreement to the data could be found using

$$D = 6.0 \times 10^{-8} S^{0.5} [m/A]^{0.7} V^2 \quad (2)$$

where D is the penetration depth in meters, S is the penetrability index, m is the mass of the penetrator in kg, A is cross-sectional area, and V is the impact speed. Here the mass of the forebody is 0.67 kg. It should be pointed out that although V^2 gave the best fit, and indeed harkens to the earliest penetration equations [*Robins*, 1742], the speed range of the tests was small, so other exponents may provide acceptable fits. Indices on the other terms might similarly find other best fit values if additional tests spanning wider parameter ranges were performed. No consistent dependence of penetration depth on impact incidence or angle of attack was found.

Different projectile shapes and speeds will give different weights to the various target properties; a higher speed impact applies greater weight to the target density, whereas low-speed penetration (such as the penetrometer used to measure *S*) is more significantly affected by target strength. Similarly, a sharp, slender penetrator may suffer more from frictional forces along its body, whereas a short, blunt one will be more sensitive to target bearing strength and density. Thus the nonunity exponent on the *S* term above should not be a great surprise.

A zeroth-order data reduction would use the accelerometry record to determine the depth of penetration, then an equation like that above to determine the depth-averaged surface hardness *S* [*Moersch and Lorenz*, 1998]. A first step is to forward model the penetration event and attempt to reproduce the flight data. One numerical code available to perform this task is the Simplified Analytical Model of Penetration with Lateral Loading (SAMPLL) from Sandia National Laboratory [*Young*, 1992]. The code takes penetrator design parameters, initial conditions at impact, and *S* values for homogeneous or layered targets and provides predicted penetrator paths and decelerations as a function of time. Ideally, a combination of more physical soil properties such as density and shear strength may be inferred. The cavity-expansion model [e.g., *Forrestal and Luk*, 1992], which is now gaining more widespread application, may be useful.

In April of 1999 a second set of air gun tests was carried out at the EMRTC with the specific objective of obtaining accelerometry data representative of the data expected to be returned from the flight probes [*Lorenz et al.*, 1999b]. Seven shots were attempted; of these, three provided useful acelerometry records of penetration into clay targets of intermediate hardness. Double integration of these data (Figure 7) using measured impact velocities gives penetration depths within ~10 cm of depths measured with a tape measure at the impact site (Figure 8). Shots into soft targets and layered targets with soft upper layers failed to provide useful accelerometry data – the forebodies in these shots failed to separate and the probes skipped out of the target. This problem was the consequence of using test probes that had smaller, heavier aftbodies and lighter forebodies than the flight probes, all of which work to inhibit separation. Future tests should rectify this problem and provide accelerometry data for softer targets. We intend to explore these aspects, and verify the detectability of target layering at impact speeds of 200 m/s with a further short series of impact

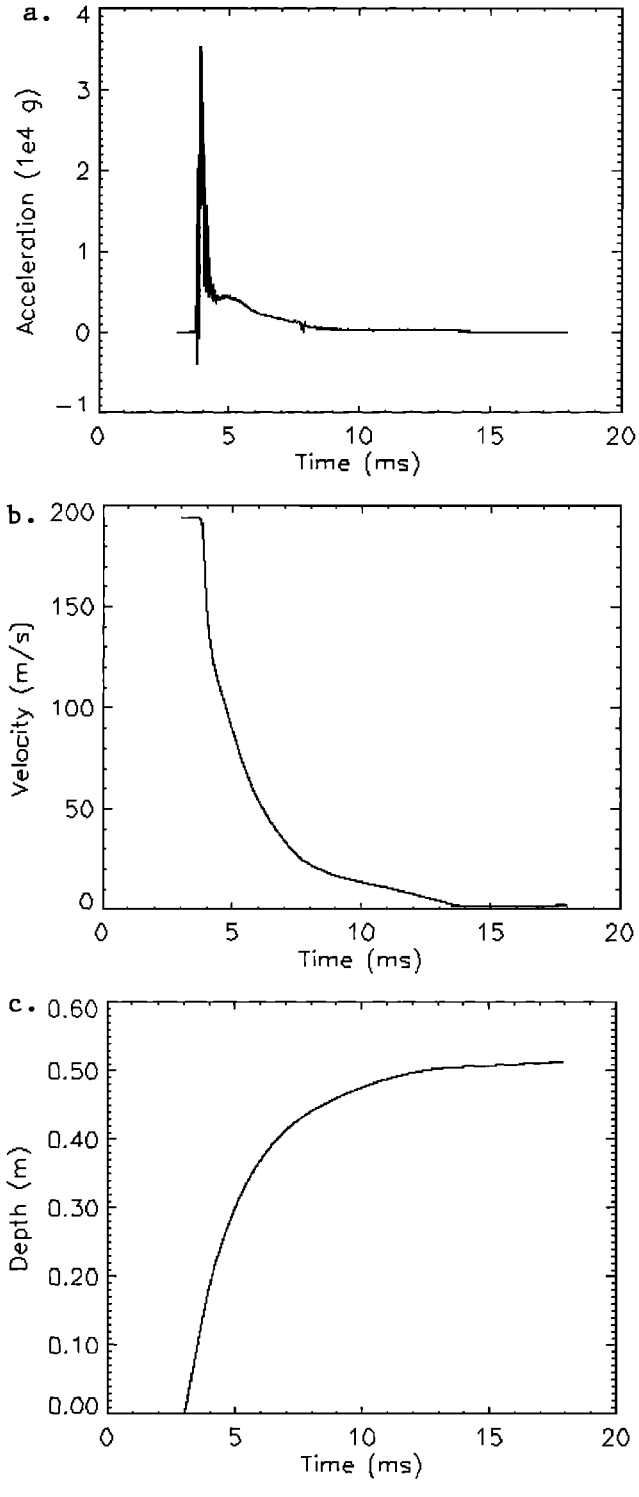

Figure 7. Z axis accelerometry record for an air gun test firing of a DS2 mock-up into a clay target of (a) intermediate hardness, and (b) the single and (c) double integrations of this record to yield a profile of velocity and depth for the impact event.

tests at EMRTC. For these experiments, a set of three orthogonal accelerometers will be mounted in the penetrator forebody, to aid in characterizing the errors associated with lateral accelerations during impact.

A third series of tests is under way [*Lorenz*, 1999] using a smaller air gun, capable of vertical impacts at up to about 50 m/s, at the University of Arizona. Although at lower impact speeds than for flight, the rapid turnaround of tests (several per day) and the ability to closely control the target stratigraphy enable these tests to provide valuable information. These tests use a piezoelectric accelerometer sampled at 10 kHz mounted in a steel slug with the same mass and dimensions as the DS2 forebody. The slug is accelerated, mounted in an aluminum sabot acting as a free piston, down a ~2 m length of 8 cm steel tubing.

These lower-speed tests indicate that layers with spacing of 5-10 cm can be resolved. The limitation is probably the nose diameter, which averages soil forces over several centimeters, rather than the number of samples per centimeter, which is a factor ~2 poorer in flight than in these tests. Fine structure in the accelerometer record may indicate structure at the centimeter level. Laboratory tests [*Lorenz et al.*, 1999b] indicate that a high-frequency noise component is found in coarse gravel targets that is not present in finer-grained materials. Another observation that has been made in these tests is that paint applied to the forebody is, in general, only abraded away on the hemispherical nose. Thus for this blunt and relatively short forebody shape, sidewall friction is evidently a minor component of the decelerating force.

4.3. Evolved Water Experiment

4.3.1. Science and technology objectives. The primary objective of the sampling/water experiment is to demonstrate a subsurface sample collection technology that will be generally applicable to future in-situ experiments on Mars. The secondary objective of this investigation is to identify and quantify the presence of water ice at the landing sites and to apply this measurement to models of the climate record and water inventory of Mars.

Constraints established by the DS2 evolved water experiment will allow the development of improved numerical models to simulate annual cycles of volatile exchange with the regolith. Such models, which would include hydrodynamic transport code [*Haberle et al.*, 1997; *Houben et al.*, 1997] as well as a rigorous boundary layer/soil model [*Zent et al.*, 1993; *Jakosky et al.*, 1997], will enhance our understanding of the surface-atmosphere interactions. Furthermore, DS2 data can be used to update local, regional, and annual models of regolith-

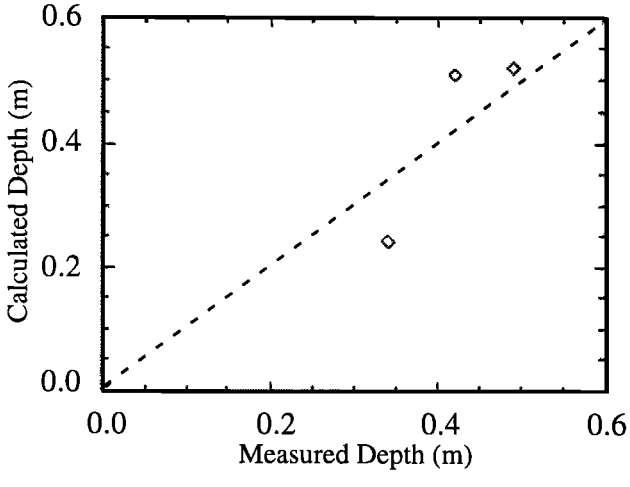

Figure 8. Comparison of penetration depths calculated via double integration of measured accelerometry versus measured depths of penetration.

atmosphere exchange at different orbital geometries where the greatest uncertainty is the behavior of the polar caps as a function of obliquity [e.g., *Kieffer and Zent*, 1992].

4.3.2. Instrument description. The instrumentation to pursue the scientific and technology objectives listed above consists of hardware for sample collection, thermal analysis, and laser spectroscopy.

4.3.2.1. Sample collection: Sample collection is achieved with an ~0.9 W electric drill mechanism that is activated after impact. The first three turns of the motor release the latches for the drill bit and for the cover that protects the openings during the impact. During the subsequent 5 min of operation, two springs are used to push the bit into the soil surrounding the forebody. The bit extends 1 cm and can deliver enough material to fill the sample cup (160 mL). After the drilling operation, a pyrotechnic actuator is activated to seal the soil chamber and to prevent the unwanted escape of evolved gases during sample analysis.

4.3.2.2. Thermal analysis: A resistive heater consisting of nichrome wire windings around the soil cup can heat the sample from ambient subsurface temperatures through the sublimation point of water ice. Current is supplied to the heater circuit directly from the batteries to eliminate the energy losses resulting from power regulation. Thermal analyses of the soil sample during heating and cool down are based on data collected from two silicon diode temperature sensors located inside the soil cup: One is on the side wall, and the second is attached to a thermally insulating (torlon) post in the center of the cup. These temperature sensors are also used for the feedback loop that controls the rate of sample heating. Gases evolved from the sample during heating are vented through four, 500 μm holes in the central post into the spectral analysis chamber located beneath the sample cup.

4.3.2.3. Laser spectroscopy: As the evolved water vapor expands into the analysis chamber, spectroscopic analyses are conducted using a tunable diode laser (TDL) scanning across a single water line in the 1.37 μm region of the spectrum. A thermally controlled substrate maintains the laser temperature within 0.2°C of the operating temperature (~10°C). The current ramp, which scans the laser across several wavenumbers, is modulated with a small 5 kHz sinusoid. Detection of the water line absorption is made at twice this modulation frequency. This technique reduces noise and increases sensitivity. The water vapor abundance in the chamber during each scan is calculated using Beer's law, the recorded direct and harmonic absorption spectra, the laser path length (2.6 cm), and the modulation parameters [*May and Webster*, 1993].

4.3.3. Experiment description. The experimental sequence is preprogrammed and consists of five parts: checkout, empty cup analysis, sample acquisition, sample verification, and ice detection.

4.3.3.1. Checkout: After separation from the carrier and prior to impact, checkout data are obtained from the experiment in a short (~20 s) sequence to verify the survival of the instrument during cruise to Mars. Laser scans, laser temperatures, and soil cup temperatures are collected and stored for downlink to assess the health of the hardware.

4.3.3.2. Calibration and sample acquisition: Two to 8 hours after impact (depending upon the battery temperatures and the timing of the first downlink pass) and before a sample is collected, an in situ calibration of the instrument thermal properties and the laser performance will be conducted. In this sequence the empty sample cup is heated at a rate of 1°C/s until its outer temperature sensor has been raised 60°C or until -10°C has been reached (whichever is lower). The two cup temperatures are sampled at 1 Hz during this heating ramp and during the first 40°C of the subsequent cool down. Direct and demodulated laser signals are collected prior to heating, at the peak temperature, and after a 40°C cool down to establish the postimpact performance.

After the 40°C cool down from the peak temperature or after 4 min (whichever is shorter), the drill motor is activated for 5 min to acquire the soil sample. Immediately after sample acquisition, the pyrotechnic actuator is activated to seal the soil cup with a titanium plate.

4.3.3.3. Sample verification: After allowing 1 hour for the instrument to cool to ambient temperatures, the empty cup analysis sequence described above is repeated for the full cup. As the outer temperature sensor is heated to match a 1°C/s ramp rate, the heat capacity of the collected sample will retard the heating rate of the inner temperature sensor relative to the empty cup. The heater voltage, as well as the duty cycle during the heating ramp, are collected during this sequence, so the energy required to heat the chamber can also be calculated and compared to the corresponding value for the empty cup. Furthermore, the cooling rate of the empty cup will be greater than with sample. Thus the heating and cooling curves as well as the energy consumption data will be used to verify that a sample was, in fact, collected. As described above, demonstration of subsurface sample collection is the primary technology objective of this instrument.

4.3.3.4. Ice quantification: The sample verification sequence will be followed by a heating profile which elevates the inner (cooler) temperature sensor to +10°C, above the sublimation point of ice, and maintains that temperature for ~4 min. Throughout this heating profile and during the subsequent 2 min of cool down, sample cup temperatures will be recorded at 1 Hz.

The temperatures and heater power data collected during this portion of the sequence should reflect sample cooling when the cup temperature is high enough to sublimate collected water ice. As the outer cup temperature sensor is driven at a rate of 1°C/s, the inner cup temperature sensor is expected to exhibit a slope change as the latent heat of vaporization takes effect. When the ice sublimates, a larger rate of energy consumption is required to maintain the programmed heating ramp, so the presence of ice should also be evident in the heater duty cycle. The duration and magnitude of the temperature and duty cycle fluctuations will be compared against the laboratory calibration data to determine the quantity of ice present in the sample. If water ice is present, spectroscopic data collected versus temperature can be used to confirm the release of water at 0°C. The lower limit for the quantity of water ice detectable by these thermal techniques will be established in the laboratory calibration work. If the quantity of ice is smaller than the thermal detection limit, a binary "yes/no" presence of water ice in the sample can still be determined from the spectroscopic data.

4.3.3.5. Calibration activities: Laboratory experiments using breadboard versions of the water experiment and electronics are ongoing to establish sensitivity limits and to provide comparisons for flight data. Soil samples of various quantities, grain sizes, composition, packing density, and ice content are introduced to a breadboard science block, cooled to Martian temperatures, pumped and backfilled with carbon dioxide at Martian pressures, and subjected to the flight sequence. Soil cup temperature profiles such as those shown in Figure 9

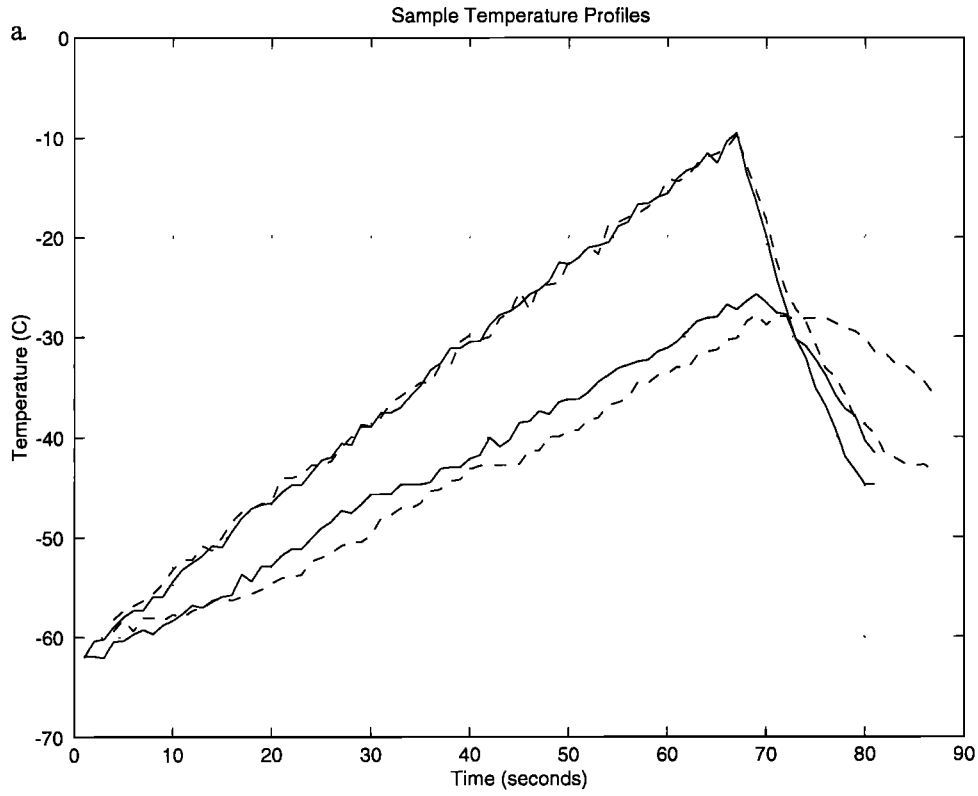

Figure 9a. Temperature profiles for an empty cup (solid lines) and for a cup full of powdered basalt (dashed lines). The lower curve in each set represents the temperature of the sensor mounted in the center of the cup, while the upper curve reflects data from a sensor at the cup wall. As the cup wall is driven at ~1°C/s, the presence of sample is evident in the different heating and cooling rates of the inner temperature sensor.

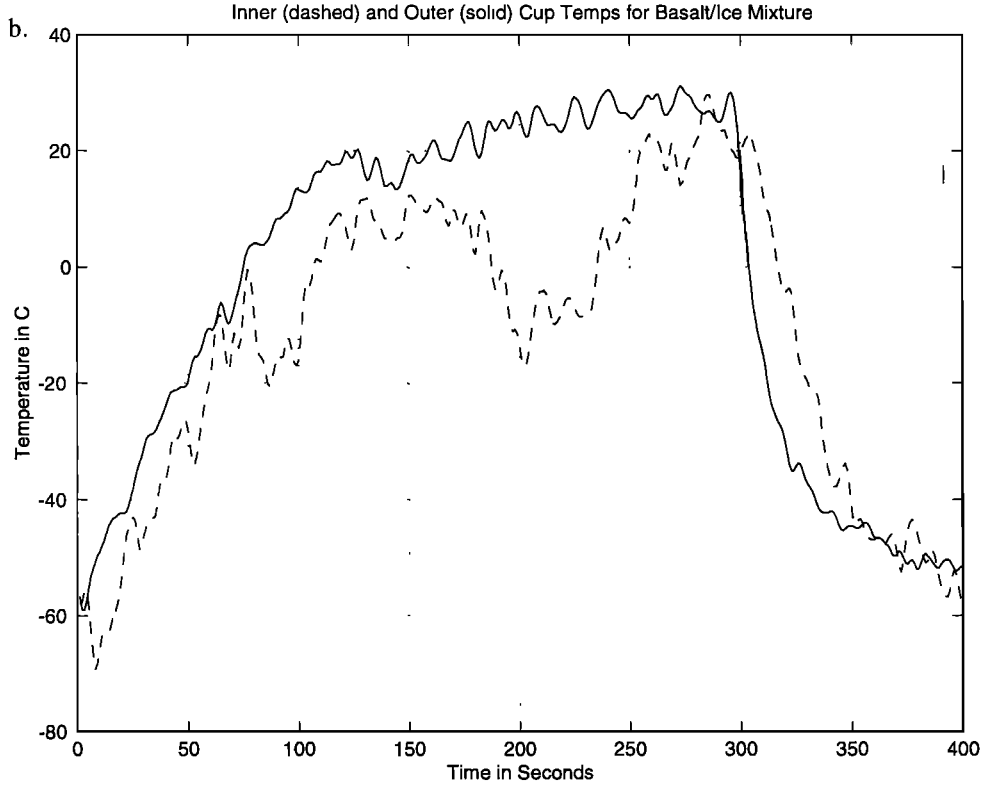

Figure 9b. Soil inner (dashed) and outer (solid) cup temperatures during heating of a mixture containing basalt and ice under Mars-like temperatures and atmospheric pressure. Two broad cooling pulses from the sublimation of ice are apparent.

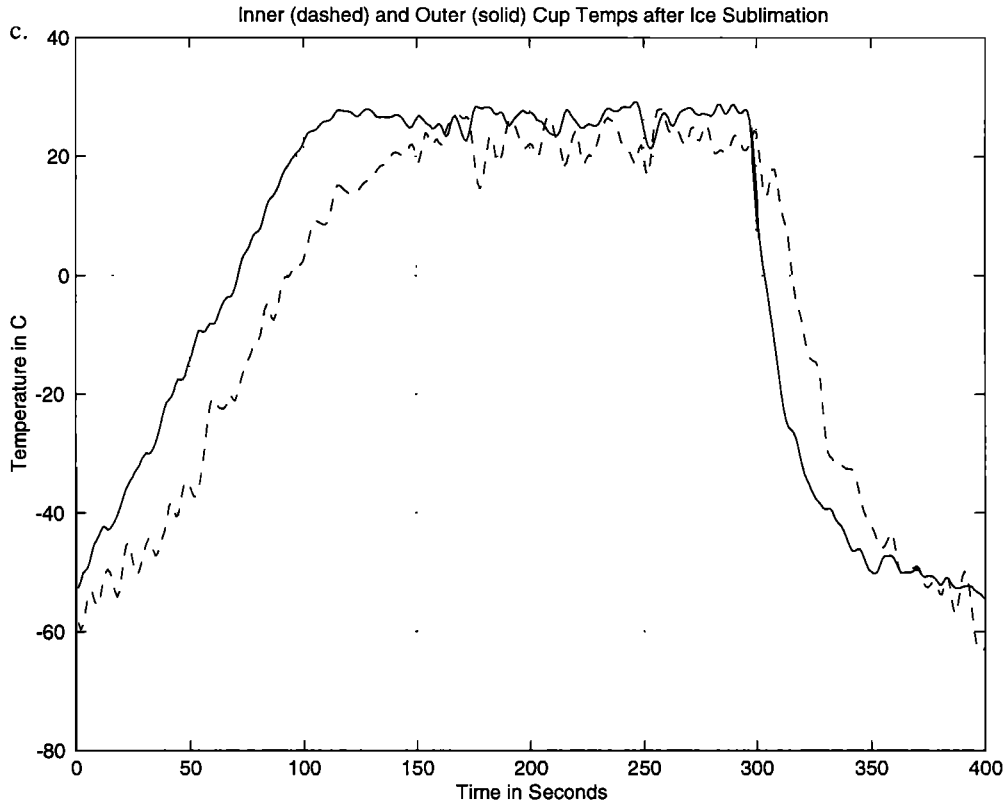

Figure 9c. A repeat of the thermal profile shows no evidence of ice.

are collected to characterize the thermal behavior for samples with different physical properties and ice contents. Ongoing laboratory experiments will allow us to address uncertainties in the source, sink, and transport rates of water vapor in this experiment. This laboratory database will be used to assist in the interpretation of data returned from Mars.

4.4. Soil Conductivity Experiment

4.4.1. Science objectives. The Soil Conductivity Experiment will provide measurements of the subsurface temperatures as the probes cool down from the heat of the impact. The primary objective is to use the cooling history to estimate the thermal conductivity of the subsurface materials. Physical parameters of the subsurface materials, such as particle size, packing density, salt cementation, can be estimated through comparison with laboratory experiments that relate thermal conductivity of particulate materials to their physical parameters. This information will provide insight into the geologic history of the polar layered terrains.

A volatile-free dust layer, with particles less than 30 μm, is extremely insulating under Martian atmospheric pressures, as such a layer would have a thermal conductivity of less than 0.02 W / mK [*Presley and Christensen*, 1997a]. Slightly higher thermal conductivities, around 0.035-0.05 W / mK, might indicate a larger particle size of 100-250 μm [*Presley and Christensen*, 1997a], the presence of cementation by salt or ice, or some combination of these factors. Since the polar layered terrain is thought to be composed primarily of dust-sized particles and some fine sand [*Herkenhoff and Murray*, 1990a], thermal conductivities above 0.05 W / mK probably would be most consistent with the presence of ice. In this case, though, particles greater than 250 μm may not be ruled out from thermal conductivity values alone.

4.4.2. Instrument description. The Soil Conductivity Experiment consists of two platinum resistor temperature sensors that will provide repeatability and linearity of the data over the temperature ranges expected. The two sensors are placed ~6 cm apart on the inner metal surface of the probe forebody. One sensor is located immediately behind the hemispherical tungsten nose, and the other is located close to the rear edge (Plate 1). If thermal equilibrium is reached, the two sensors will allow for interpretation of any spatial thermal gradients induced either by the geometry of the probe or by small-scale layering of the subsurface materials.

4.4.3. Experiment description. Material thermal properties, such as thermal conductivity and thermal diffusivity, are routinely measured in the laboratory using either steady state heat flux or transient heating methods [*Beck*, 1988]. Most field applications of these techniques use the thermal decay from a calibrated heat pulse [*Beck*, 1988]. The disadvantage of these techniques for the microprobe application, however, is the requirement of a power supply for the calibrated heat pulse. Therefore we have developed methods that do not require a calibrated heat pulse.

Energy is available from two sources as the microprobe enters the ground: kinetic energy from the velocity of the probe and thermal energy from the heat capacity of the probe due to the probe-regolith temperature difference at the time of penetration. Kinetic energy released by the probe on impact from a velocity of 200 m/s is 20,000 J per kg of probe mass. Theoretical and field studies indicate that half of the energy is converted to thermal energy [*Pitts and Canning*, 1976; *Blanchard et al.*,

1976]. Thus for the probe mass of 0.67 kg, the predicted energy from the impact event should be ~13 kJ. Assuming that the main mass of the probe is metallic, the heat available by virtue of the difference in temperature of the probe and the regolith is roughly 400 J per kg of probe mass per °C of temperature difference between the probe and the regolith. Conversion of half the impact energy to a temperature increase results in a temperature increase of ~17°C. This approximate value is consistent with field studies conducted on prototypes of DS2. The temperature of the probe on impact will be between -40° and -20°C. The predicted subsurface temperature at a depth of 0.3 to 1 m is between -70 and -110°C, depending on the ice content and thermal conductivity of the soil. Assuming 17°C of impact heating, the temperature difference between the probe and the surrounding material is predicted to be in the range of ~ 47° and 107°C. For this temperature range the predicted thermal energy difference is between 13 and 29 kJ. The decay of this thermal energy will be easily resolved.

Analytic solutions exist for a cooling cylindrical probe [*Bullard*, 1954; *Jaeger*, 1956; *Carslaw and Jaeger*, 1959] and are commonly used for thermal probes penetrating oceanic sediment. The ratio of the temperature of the surface of the probe T_t at time T and its initial temperature T_0 at time $t = 0$ is given by a function known as the F function:

$$\frac{T_t}{T_0} = F(\alpha, \tau)$$

where

$$\alpha = \frac{2\pi a \rho \sigma}{m} \qquad \tau = \frac{\kappa t}{a^2}$$

and a is the probe radius, ρ, σ, and κ are the density, specific heat, and thermal diffusivity of the regolith, and m is the heat capacity of the probe. The F function is a nonlinear integral of Bessel functions with arguments defined by the variables in α and τ and tables of this function are published for different values of its arguments [e.g., *Jaeger*, 1956]. The magnitude of the initial heat pulse is normally required in order to determine the initial temperature of the probe for the solution of this problem. However, using thermal relaxation data from the air gun tests, an iterative scheme was demonstrated to be able to find the best initial probe temperature and regolith parameters in order to produce an acceptable fit to the observed data. The parameters thus determined were compared with published data and found to be reasonable estimates of the regolith properties.

In addition to the analytic solutions described above, a finite difference solution that models the specific geometry of the DS2 probe has been developed. This model provides an excellent fit to laboratory thermal calibration data for the microprobes and will be used to interpret the data returned from Mars, including uncertainties in the conductivity estimate.

Several properties of the Martian surficial material determine the bulk thermal conductivity that will be measured by the Mars microprobes. These properties include particle size and shape, bulk density, cementation of the particles by salt, subsurface layering, and ambient temperature. Characterization of surficial material from its thermal conductivity requires some knowledge of the magnitude of these effects.

A comprehensive laboratory study on the effects of particle size on thermal conductivity has been done [*Presley and Christensen*, 1997a]. Preliminary studies were also done on the effects of particle shape and bulk density of particulate materials over a range of atmospheric pressures [*Presley and Christensen*, 1997b]. From these experiments, particle shape appears to affect thermal conductivity primarily through the control of the bulk density of the deposit. Although the thermal conductivity of materials made up of conchoidally shaped particles have been measured previously, [*Wechsler and Glaser*, 1965; *Smoluchowski*, 1910; *Woodside and Messmer*, 1961; *Bernett et al.*, 1963; *Presley and Christensen*, 1997c], particle shape and bulk density effects have not been separated. Furthermore, the effect of flat particle shapes, as found in clay-rich sediments, also has not been investigated. Clearly, laboratory measurements of other, more complex natural surfaces would be valuable in order to interpret the thermal conductivity measured in terms of the physical properties of the surficial materials.

5. Synergy Between Experiments and Other Mars Missions

5.1. Subsurface Measurements

The science return from Mars will be amplified by the redundancy of measurements at two separate sites in addition to the comparisons to the more advanced and complete measurement set made by the Mars Polar Lander. The objective is to apply the results of the mission to our understanding of the Martian climate and geologic record. The data sets described above will constitute a ground truth characterization of materials in the layered terrain and, as such, can be used to improve models of layered terrain formation, regolith-water interactions, and the role of the layered terrain in the Martian climate history.

The initial analysis will determine the variability of the small-scale stratigraphic structure between sites. Next, the information from the water, soil conductivity, and impact experiments will be examined to attempt to better constrain the derived soil properties. All of the probe in situ measurements are related to the amount of ice present in the subsurface. Significant percentages of water ice, ~5-10% and perhaps even less, will both dramatically increase the hardness of the soil detected by the impact accelerometer and will cause an increase in the soil conductivity of an order of magnitude or more. In general, the lower the thermal conductivity of a material, the lower its bulk density and the softer the material. The accelerometer data can be investigated to look for layering that might represent ice, or the presence of a poorly consolidated layer of aeolian dust near the surface [e.g., *Paige*, 1992]. In addition, the estimate of sample depth must come from the accelerometer. The impact velocity will be determined from the trajectory reconstructed using the descent accelerometer data and will be of use in the evaluation of the penetration depth from the impact accelerometer data. Additionally, it will be possible to use the results of the thermal conductivity experiment to estimate the product of the thermal conductivity and density of the regolith. By combining the evolved water experiment analysis with the bulk conductivity estimates, the uncertainty with respect to ice content can be reduced, and the residual thermal signature of the refractory materials explored [*Presley and Christensen*, 1997a,c].

A more complete evaluation of the regional variability of the geologic record in the polar layered terrain will come from comparison of the two environmental characterizations with each other, and with the Mars Polar Lander data. The Mars Volatile and Climate Surveyor (MVACS) payload (D. A. Paige et al., submitted paper, 1999) on the Mars Polar Lander carries

experiments that provide parallel information for all of the experiments on DS2. The Thermal Evolved Gas Analysis (TEGA) instrument (W. Boynton et al., The Mars Volatile and Climate Surveyor Thermal and Evolved-Gas Analyzer, submitted to *Journal of Geophysical Research,* 1999) will use both differential scanning calorimetry and evolved gas analysis to search over the depth accessed by the robotic arm for water ice, water adsorbate in ice-free samples, carbon dioxide, and selected refractory minerals. The arm camera will acquire imagery of the samples in situ. The robotic arm (R. G. Bonitz et al., MVACS robotic arm, submitted to *Journal of Geophysical Research,* 1999) will also characterize the physical properties of the near-surface regolith as it digs. This information on the properties at exact depths below the surface will be compared to the DS2 impact accelerometer data. MVACS will also measure soil thermal properties at a depth of several centimeters using a thermal probe on the robotic arm (S. E. Wood and D. A. Paige, The MVACS soil temperature probe, submitted to *Journal of Geophysical Research,* 1999). Comparison of the near-surface thermal properties with those at 0.2 to 0.6 m will determine any changes over depth.

Orbital data will also be examined to characterize the heterogeneity of the landing sites, their thermophysical and morphological properties at scales substantially larger than those available to the landed spacecraft, and to correctly place the sample data and subsequent environmental analyses in their geologic and stratigraphic context. MGS is currently collecting data that will be of value in interpreting the data returned by DS2. The Mars Orbital Camera on MGS will be imaging the landing sites for the microprobes and the Polar Lander at a resolution of 2-3 m. The Mars Observer Laser Altimeter has mapped the local topography in detail. Higher resolution TES data will also be available for the region prior to impact.

5.2. Atmospheric Measurements

The close proximity of the Mars Microprobe impact sites to the landing site of the Mars Polar Lander offers a unique opportunity for a coordinated investigation of the atmosphere. Onboard accelerometers on the Mars Polar Lander will measure the deceleration of the lander to determine the timing of the start of the parachute descent phase. A small subset of this data will be stored and returned to Earth for an investigation of atmospheric structure. Thus the first opportunity to study the horizontal variability between three atmospheric structure profiles acquired within ~50 km of each other will be created. The returned data from the Mars Microprobe Mission will offer higher vertical resolution and will enable derivation of atmospheric structure below the Mars Polar Lander's parachute release altitude of ~14 km. The Meteorology Experiment on the Mars Polar Lander (D. Crisp et al., submitted paper, 1999) will characterize the surface meteorology by measuring near-surface atmospheric temperatures, atmospheric pressure, winds, and humidity. The atmospheric temperature profiles derived from the Mars Microprobe ADA experiment will allow an extension of the Mars Polar Lander observations of near-surface temperature and pressure to ~75 km altitude at two nearby locations.

The atmospheric light-detection and ranging (LIDAR) experiment on the Polar Lander (S. Linkin and S. Lipatov, The LIDAR experiment on the Mars Polar Lander, submitted to *Journal of Geophysical Research,* 1999) will determine the altitude of dust hazes and ice clouds above the landing site within the lowest few kilometers. The signature of dust and cloud opacity is potentially visible in the atmospheric temperature profiles as heating due to increased absorption of sunlight by dust or enhanced radiative cooling produced by cloud opacity. In addition, by neglecting horizontal variability between the landing sites, the atmospheric structure profiles from the ADA can potentially provide information on the atmospheric temperatures associated with clouds or fogs observed by the LIDAR. As a result, determination of the saturation temperature of clouds and fogs and hence the water mixing ratios associated with the clouds may be possible. Therefore the atmospheric science measurements from the Mars Polar Lander and from the Mars Microprobe Mission provide highly complementary information, which can yield valuable constraints on processes in the polar atmosphere of Mars.

The Mars Microprobe Mission atmospheric structure profiles will also uniquely complement remote sensing observations of atmospheric temperatures from the MGS orbiter. The better than 1 km vertical and horizontal resolution of the atmospheric structure profiles from the ADA provide the only means of characterizing atmospheric phenomena with vertical and horizontal scales smaller than 10 km. The Thermal Emission Spectrometer (TES) on MGS [*Christensen et al.*, 1998] will provide regional and global determinations of temperature on larger than 10 km horizontal scales and 5-10 km vertical scales. Observations of the Mars Polar Lander and Mars Microprobe landing areas near the time of the probe entries would be particularly valuable. Such measurements will allow the temperature profiles from the microprobes to be placed in a regional and seasonal context. In particular, horizontal variability between the Mars Polar Lander and Mars Microprobe sites can be assessed and considered when comparing atmospheric measurements from these three probes.

6. Data Management

Science data returned from DS2 will be archived by the project and the science team in NASA's Planetary Data System. The data will be archived together with that of the Mars Polar Lander. Due to the technology demonstration objectives of DS2, as many engineering data as are practical will also be incorporated with the science data. There is no proprietary period for any data, and the project encourages rapid dissemination of the data. However, the data must be validated and calibrated prior to release. This work will be performed in 6 months or less.

7. Discussion and Summary

The primary objective of DS2 is to demonstrate numerous new technologies that allow extremely small landed payloads to carry out surface and subsurface science. In addition to the network science missions that require many small distributed landers, the experiments carried on this mission may serve as precursors to a variety of other future missions. The demonstration of the soil sampling mechanism and water detection with a TDL have inspired designs of a several other types of soil analysis [e.g., *Yen et al.*, 1999]. Impact accelerometers are essential for all penetrators to determine the depth of penetration. The integration of the data from the two probes and the robotic arm on the lander will provide an excellent validation of the penetrator-based approach to characterizing subsurface materials. The DS2 Mars Microprobe Mission will demonstrate the

facility of determining the thermal conductivity. The heat flux at the surface is a product of the vertical thermal gradient and the soil conductivity. A future network of dozens of similar probes with the ability to measure thermal gradient thus would allow the determination of the internal heat flow contribution to the heat flux through the elimination of the diurnal and seasonal contributions, as well as the effects of the thermal properties of the subsurface materials. Knowledge of the internal heat flow of Mars would provide a better understanding of its present state of volcanic and tectonic activity.

The secondary objective for the mission is to collect valuable science data. The data from the descent accelerometer will constrain the atmospheric density, pressure, and temperature at a new latitude and a new season. The data can be collected all the way to the surface for the first time because of the entry system design. Even more exciting is the ability to determine small-scale variations in the atmospheric structure through comparison of the two entry profiles from DS2 and possibly a third profile from the Mars Polar Lander. Data from each of the in situ measurements, the evolved water experiment, the soil conductivity experiment, and the impact accelerometer should dramatically improve our understanding of the variability and properties of the polar layered terrain. The ability to compare the information obtained from DS2 with that from the MVACS payload at a different location on the polar layered terrain, as well orbital characterizations of the landing site, greatly enhances the science return from the three in situ experiments.

Acknowledgments. The Mars Microprobe Project, and in particular, Sarah Gavit, George Powell, Randy Blue, and Kari Lewis, deserves acknowledgment for accomplishing a task that was not infrequently viewed as impossible by some outside the project. Suzanne Smrekar is the project scientist; Diana Blaney is also on the DS2 project staff. Other authors constitute the science team. This paper was substantially improved due to reviews by Jim Bell and an anonymous reviewer.

References

Banerdt, W., W. Kaiser, and T. Van Zandt, A microseismometer for terrestrial and extraterrestrial applications, Workshop on Advanced Technologies for Planetary Instruments, *LPI Tech. Rep,. 93-02*, Part 1, 1, 1993.

Barnes, J. R., Possible effects of breaking gravity waves on the circulation of the middle atmosphere of Mars, *J. Geophys Res., 95*, 1401-1421, 1990.

Beck, A. E., Methods for determining thermal conductivity and thermal diffusivity, in *Handbook of Terrestrial Heat-Flow Density Determination,* edited by R. Haenel, L. Rybach and L. Stegena, pp. 87-124, Kluwer Acad., Norwell, Mass., 1988.

Bernett, E. C., H. L. Wood, L. D. Jaffee, and H.E. Martens, Thermal properties of a simulated lunar material in air and in vacuum, *Am Inst. Aeronaut. Astronaut. J., 1*, 1402-1407, 1963.

Blanchard, M. B., V. R. Oberbeck, T. E. Bunch, R. T. Reynolds, T. N. Canning, and R. W. Jackson, FY 1976 progress report on a feasibility study evaluating the use of surface penetrators for planetary exploration, *NASA Tech. Memo. X-73,*181, 1976.

Braun, R. D, R. A. Mitcheltree, and F. M. Cheatwood, Mars microprobe entry-to-impact analysis, *J. Spacecraft Rockets, 36*, 392-398, 1999.

Bullard, E. C., The flow of heat through the floor of the Atlantic Ocean, *Proc. R. Soc. Lond, Ser., A, 222*, 403-429, 1954.

Carslaw, H. S., and J. C. Jaeger, *Conduction of Heat in Solids*, 510 pp., Oxford Univ. Press, New York, 1959.

Christensen, P. R., et al., Results from the Mars Global Surveyor Thermal Emission Spectrometer, *Science, 279*, 1692-1698, 1998.

Forrestal, M. J., and V. K. Luk, Penetration into soil targets, *Int. J Impact Eng. 12*, 427-444, 1992.

Garry, J., Going underground, *New Sci.*, pp. 44-47, Nov. 22, 1997.

Gavit, S. A., and G. Powell, The New Millennium Program Mars Microprobe Mission, *Acta Astronaut. 39*, (1-4), 273-280, 1996.

Haberle, R. M., J. B. Pollack, J. R. Barnes, R. W. Zurek, C. B. Leovy, J. R. Murphy, H. Lee, and J. Schaeffer, Mars atmospheric dynamics as simulated by the NASA Ames general circulation model, 1, The zonal-mean circulation, *J. Geophys Res., 98*, 3093-3123, 1993.

Haberle, R. M., H. Houben, J. R. Barnes, and R. E. Young, A simplified three-dimensional model for Martian climate studies, *J Geophys Res., 102*, 9051-9067, 1997.

Haberle, R. M., et al., General circulation model simulations of the Mars Pathfinder atmospheric structure investigation/ meteorology data, *J Geophys. Res , 104*, 8957-8974, 1999.

Herkenhoff, K. E., and B. C. Murray, Color and albedo of the south polar layered deposits on Mars, *J. Geophys Res., 95*, 1343-1358, 1990a.

Herkenhoff, K. E., and B. C. Murray, High-resolution topography and albedo of the south polar layered deposits on Mars, *J. Geophys Res., 95*, 14,511-14,529, 1990b.

Hofstadter, M. D., and B. C. Murray, Ice sublimation and rheology: Implications for the Martian polar layered deposits, *Icarus, 84*, 352-361, 1990.

Houben, H., R. M. Haberle, R. E. Young, and A. P. Zent, Modeling the Martian seasonal water cycle, *J. Geophys. Res , 102*, 9069-9083, 1997.

Ivanov, A. B., and D. O. Muhleman, Topography of the north and south polar ice caps on Mars, in *Fifth International Mars Conference* [CD-ROM], *LPI Contrib. 972*, abstract 6188, Lunar and Planet. Inst., Houston, Tex., 1999.

Jaeger, J.C., Conductivity of heat in an infinite region bounded internally by a cylinder of a perfect conductor, *Aust. J Phys., 9*, 167-179, 1956.

Jakosky, B. M. and R. M. Haberle, The seasonal behavior of water on Mars, in *Mars*, edited by H. Kieffer, B. Jakosky, C. Snyder, and M. Mathews, pp. 969-1016, Univ. of Ariz. Press, Tucson, 1992.

Jakosky, B. M., A. P. Zent, and R. W. Zurek, The Mars water cycle: Determining the role of exchange with the regolith, *Icarus, 130,* 87-95, 1997.

Kieffer, H. H., and A. P. Zent, Quasi-periodic climate change on Mars, in *Mars*, edited by H. Kieffer, B. Jakosky, C. Snyder, and M. Mathews, pp. 1180-1218, Univ. of Ariz. Press, Tucson, 1992.

Lorenz, R. D., Penetrator experiments with the UA Airgun in support of DS-2 and future missions paper presented at Mars Exploration Programme and Sample Return Missions, NASA/CNES Paris, Feb. 1999.

Lorenz, R. D., J. E. Moersch, S. E. Smrekar, R. M. Keaton, and J. A. Stone, Impact penetration of the DS-2 Mars Microprobes, *Lunar Planet. Sci.* [CD-ROM]. *XXX*, abstract 1042, 1999a.

Lorenz, R. D., J. E. Moersch, J. A. Stone, A. R. Morgan, and S. E. Smrekar, Penetration tests on the DS-2 Mars microprobes: Penetration depth and impact accelerometry, *Planet. Space Sci.*, in press, 1999b.

Magalhães, J. A., J. T. Schofield, and A. Seiff, Results of the Mars Pathfinder Atmospheric Structure Investigation, *J. Geophys. Res., 104*, 8943-8955, 1999.

May, R. D., and C. R. Webster, Data-processing and calibration for tunable diode-laser harmonic absorption spectrometers, *J. Quant. Spectrosc. Radiat. Transfer, 49*, 335-347, 1993.

Mellon, M. T., B. M. Jakosky, H. H. Kieffer, and P. R. Christensen, High resolution mapping of thermal inertia from Mars Global Surveyor Thermal Emission Spectrometer, in *Fifth International Mars Conference* [CD-ROM], *LPI Contrib 972*, abstract 6131, Lunar and Planet. Inst., Houston, Tex., 1999.

Mitcheltree, R. A., J. N. Moss, F. M. Cheatwood, F. A. Greene, and R. D. Braun, Aerodynamics of the Mars Microprobe entry vehicles, *J. Spacecraft Rockets, 36*, 412-420, 1999.

Mizutani, H., Lunar interior exploration by Japanese lunar penetrator mission, LUNAR-A, *J. Phys. Earth, 43*, 657-670, 1995.

Moersch, J. E., and R. D. Lorenz, Subsurface structure in the Martian polar layered deposits: The DS-2 impact accelerometer experiment, First International Conference on Mars Polar Exploration, *LPI Contrib., 953*, 27, 1998.

Muhleman, D. O., B. J., Butler, A. W. Grossman, and M. A. Slade, Radar images of Mars, *Science, 253*, 1508-1513, 1991.

Nelson, R. M., Deep Space One: Preparing for space exploration in the 21st century, *Eos Trans. AGU, 79*, 493, 496, 498, 1998.

Paige, D. A., The thermal stability of near-surface ground ice on Mars, *Nature, 356*, 43-45, 1992.

Paige, D. A., and K. D. Keegan, Thermal and albedo mapping of the south polar region of Mars using Viking thermal mapper

observations, 2, South polar region, *J. Geophys. Res., 99*, 25,993-26,014, 1994.

Paige, D. A., J. E. Bachman, and K. D. Keegan, Thermal and albedo mapping of the polar regions of Mars using Viking thermal mapper observations, 1, North polar region, *J. Geophys. Res., 99*, 25,959-25,992, 1994.

Pike, W. T., R. D. Martin, W. J. Kaiser, and W.B. Banerdt, Development of microseismometers for space applications, *Ann. Geophys., 14*, C828, 1996.

Pitts, W., and T. N. Canning, Influence of penetrator on local soil temperatures, *NASA Tech. Memo X-73*, pp. 208-217, 1976.

Pollack, J. B., R. M. Haberle, J. Schaeffer, and H. Lee, Simulations of the general circulation of the Martian atmosphere, I, Polar processes, *J. Geophys. Res., 95*, 1447-1474, 1990.

Presley, M. A., and P. R. Christensen, Thermal conductivity measurements of particulate materials, 2, Results, *J Geophys. Res., 102*(E3), 6551-6566, 1997a.

Presley, M. A., and P. R. Christensen, Thermal conductivity measurements of particulate materials, 1, A review, *J. Geophys Res., 102*(E3), 6535-6549, 1997b.

Presley, M. A., and P. R. Christensen, The effect of bulk density and particle size sorting on the thermal conductivity of particulate materials under Martian atmospheric pressures, *J. Geophys. Res., 102*(E4), 9221-9229, 1997c.

Reynolds, J. K., D. C. Catling, R. Blue, N. Maluf, and T. W. Kenny, Packaging and instrumentation of a micromachined pressure sensor for high-g impact and Martian environment, Micro-Electro-Mechanical Systems (MEMS), *ASME, DSC , 66* , 401-406, 1998.

Robins, B., *New Principles of Gunnery*, XX pp., Nourse, London, 1742.

Seiff, A., and D. B. Kirk, Structure of the atmosphere of Mars in summer at midlatitudes, *J. Geophys. Res. 82*, 4364-4378, 1977.

Smith, P. H., et al., Results from the Mars Pathfinder Camera, *Science, 278*, 1758-1765, 1997.

Smoluchowski, M.M., Sur la conductibilite calorifique des corps pulverises, *Bull Int. Acad. Sci Cacovie, 5A*, 129-153, 1910.

Stone, J. A., and T. P. Rivellini, Configuration evolution of the DS-2 Penetrator, paper presented at the 3rd IAA International Conference on Low-Cost Planetary Missions, Pasadena, Calif., April 1998.

Surkov, Y. A., and R. S. Kremnev, Mars-96 Mission: Mars exploration with the use of penetrators, *Planet. Space Sci., 46*, 1689-1696, 1998.

Thomas, P., S. W. Squyres, K. Herkenhoff, A. Howard, and B. Murray, Polar deposits of Mars, in *Mars*, edited by H. Kieffer, B. Jakosky, C. Snyder, and M. Mathews, pp. 767-798, Univ. of Ariz. Press, Tucson, 1992.

Wechsler, A. E., and P. E. Glaser, Pressure effects on postulated lunar materials, *Icarus, 4*, 335-352, 1965.

Woodside, W., and J. H. Messmer, Thermal conductivity of porous media, I, Unconsolidated sands, *J Appl Phys , 32*(9), 1688-1699, 1961.

Yen, A. S., S. E. Smrekar, and B. C. Murray, Future Mars micropenetrators based on New Millennium DS2 (DS2), *Lunar Planet Sci.* [CD-ROM], *XXX*, abstract 1870, 1999.

Young C. W., The development of empirical equations for predicting depth of an Earth-penetrating projectile, *Rep. SC-DR-67-60*, Sandia Labs., Albuquerque, May 1967.

Young, C. W., A simplified analytical model of penetration with lateral loading (SAMPLL) – An update , *Rep. SAND91-2175*, Sandia Labs., Albuquerque, 1992.

Young, C. W., Penetration equations, *Rep SAND97-2426,* Sandia Labs., Albuquerque, 1997.

Zent, A. P., R. M. Haberle, H. C. Houben, and B. M. Jakosky, A coupled subsurface-boundary layer model of water on Mars, *J. Geophys Res., 98*, 3319-3337, 1993.

Zuber, M. T., Structure of the Martian polar deposits, in *Fifth International Mars Conference* [CD-ROM], *LPI Contrib 972*, abstract 6229, Lunar and Planet. Inst., Houston, Tex., 1999.

Zurek, R. W., J. R. Barnes, R. M. Haberle, J. B. Pollack, J. E. Tillman, and C. B. Leovy, Dynamics of the atmosphere of Mars, in *Mars*, edited by H. Kieffer, B. Jakosky, C. Snyder and M. Matthews, pp. 835-933,. Univ. of Ariz. Press, Tucson, 1992.

D. Blaney, S. Smrekar, and A. Yen, Jet Propulsion Laboratory, California Institute of Technology, Mail Stop 183-501, 4800 Oak Grove Dr., Pasadena, CA 91109-8099. (blaney@sen1.jpl.nasa.gov; ssmreka@ cythera.jpl.nasa.gov; albert.yen@jpl.nasa.gov)

D. Catling, J. Magalhães, J. Moersch, and A Zent, NASA Ames Research Center, Moffett Field, CA, 94035-1000. (catling@humbabae.arc.nasa.gov, jmoersch@mail.arc.nasa.gov; zent@barsoom.arc.nasa.gov)

R. Lorenz, Lunar and Planetary Laboratory, University of Arizona, Tucson, AZ 85721-0092. (rlorenz@lpl.arizona.edu)

P. Morgan, Department of Geology, Northern Arizona University, P.O. Box 4099, Flagstaff, AZ 86011. (Paul.Morgan@nau.edu)

B. Murray, Department of Geology and Planetary Science, Mail Code 150-21, 1200 East California Boulevard, California Institute of Technology, Pasadena, CA 91125

M. Presley, Department of Geology, Box 871404, Arizona State University, Tempe, AZ 85287-1404. (mpresley@asu.edu)

(Received April 22, 1999; revised August 17, 1999;
accepted August 23, 1999.)